PSFC/JA-11-32

Characterization of the Pedestal in Alcator C-Mod ELMing H-Modes and Comparison to the EPED Model

Walk, J.R., Snyder, P.B.*, Hughes, J.W., Terry, J.L.,
Hubbard, A.E., Phillips, P.E**

* General Atomics
** University of Texas at Austin.

November, 2011

Plasma Science and Fusion Center
Massachusetts Institute of Technology
Cambridge MA 02139 USA

This work was supported by the U.S. Department of Energy, Grant No. DE-FC02-99ER54512. Reproduction, translation, publication, use and disposal, in whole or in part, by or for the United States government is permitted.

Submitted for publication to *Nuclear Fusion.*

Characterization of the Pedestal in Alcator C-Mod ELMing H-Modes and Comparison to the EPED Model

J R Walk[1], P B Snyder[2], J W Hughes[1], J L Terry[1], A E Hubbard[1], and P E Phillips[3]

[1] MIT Plasma Science and Fusion Center, 77 Massachusetts Avenue, Cambridge, MA 02139

[2] General Atomics, San Diego, CA, USA

[3] UT-Austin Fusion Research Center, Austin, TX, USA

E-mail: jrwalk@psfc.mit.edu

Abstract. A dedicated series of ELMing H-Mode discharges on Alcator C-Mod spanning a broad range of plasma parameters, including plasma current (400-1000kA), magnetic field (3.5-8T), and plasma shaping, are presented with experimental scalings of the plasma pedestal with bulk plasma and engineering parameters. The H-modes presented achieve pedestals with densities spanning $5 \times 10^{19} - 2.5 \times 10^{20}$ m^{-3} and temperatures of $150 - 1000$ eV (corresponding to $5 - 40$ kPa in the pressure pedestal), over a width of $3 - 5\%$ of poloidal flux. The observed pedestal structure is compared with the most recent iteration of the EPED class of models, which uniquely predict the pedestal width and height for a set of scalar input parameters via a combination of stability calculations for peeling-ballooning MHD modes and kinetic ballooning modes (KBM).

PACS numbers: 52.55.Fa,52.55.Tn,52.25.Fi,52.40.Hf,52.35.Py

1. Introduction

The high-confinement mode (H-mode) operational regime, first observed on the ASDEX tokamak [1], is characterized by the formation of a high-gradient region in density and temperature at the plasma edge, termed the *pedestal*. It has been shown (e.g. [2, 3, 4]) that, by inhibiting energy and particle transport across the plasma edge, the total confinement and therefore overall performance of the plasma are strongly influenced by the height and gradient of the temperature and pressure pedestal. ELMing H-modes, first characterized by Keilhacker *et al* [5], represent a hard limit on the attainable pressure pedestal height and gradient, as well as acting as a "safety valve" of sorts to vent accumulated impurities from the plasma. Therefore, an understanding of the pedestal structure in ELMing H-modes is desirable both as a potential operating scenario and as a limit on pedestal scaling for projecting future performance on ITER.

In ELMing H mode operation, the temperature and pressure pedestal gradients rise until an edge MHD instability is triggered, limiting further growth of the pedestal. Although ELM phenomenology is not fully understood, several distinct ELM types have been identified using D_α radiation observations, diamagnetic energy collapse, divertor heat loading, and phase-contrast interferometry [6]. Successful modeling of the ELM trigger event by a combination of pressure-driven ballooning modes and current-driven edge kink/peeling modes (collectively known as "peeling-ballooning" modes) has been accomplished across several machines and in a number of different operational regimes [7, 8, 9]. This motivated the development of the EPED model [9, 10], which predicts pedestal structure near the ELM stability boundary via the combination of stability calculations for the non-local peeling-ballooning modes with a calculated kinetic ballooning mode (KBM) constraint (described in section 4). This paper will investigate the application of the newest version of the model, EPED1.63, to Alcator C-Mod ELMy H modes.

2. Experimental Arrangement

2.1. ELMing Phenomenology and Plasma Operation

Edge-localized mode (ELM) phenomena cover a range of periodic perturbations of the plasma edge, generally characterized by D_α radiation spikes, diamagnetic energy collapse, and divertor heat loading [11, 6]. ELM events range from larger, slower crashes, which can expel as much as 10% of the plasma stored energy and are prevalent on DIII-D and JET [12, 7, 13], to the smaller, rapidly oscillating modes prevalent on C-Mod and other devices with high edge collisionality [14, 15, 16, 9]. The broad range of operational parameters and edge behaviors exhibited in ELMing regimes precludes a single simple driver for the modes; however, a unified analysis is still possible.

ELMing H-modes on C-Mod were achieved across a range of plasma current from 400 to 1100kA (corresponding to $\sim 0.25-0.5$ in Greenwald fraction at typical operating densities), at on-axis toroidal field values of 3.5, 5.4, and 8T (note that all low-field

shots were at lower current, while high-field discharges were at higher current). A scan in elongation over $1.45 < \kappa < 1.6$ was also achieved in an altered equilibrium conducive to ELMing operation [17] with lower elongation and upper triangularity than standard C-Mod equilibria, as shown in figure 1. All ELMing H-modes were ICRF heated, using H minority resonance for the 3.5T and 5.4T discharges, and ^{3}He minority heating for the 8T plasmas.

2.2. Diagnostics

Experimental measurements of the electron density and temperature pedestals are taken with the core and edge Thomson Scattering spectrometer systems. Two Nd:YAG lasers fired vertically through the plasma provide the scattering photons, which are collected in core and edge fibers running to a set of polychromators [18, 19]. The beam path is shown in figure 1, overlaid on C-Mod equilibria with normal and the altered shaping used for ELMing H-modes. Note that the edge fibers can be moved to optimize coverage of the plasma pedestal over the range of plasma shaping.

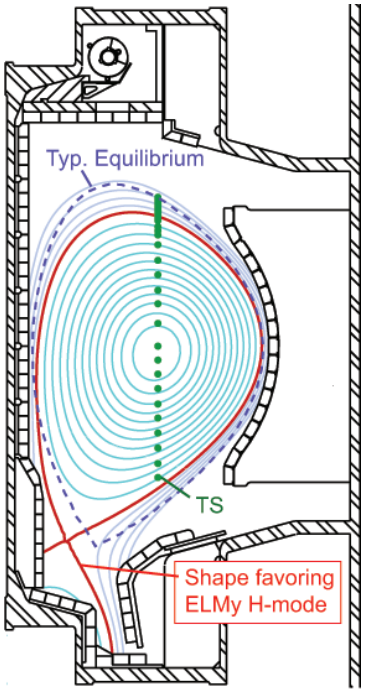

Figure 1: Vacuum-vessel cross-section showing the Thomson Scattering beam path and C-Mod equilibria. The dots indicate the positions of the core and edge TS scattering volumes, while the contours show the EFIT reconstruction of a C-Mod equilibrium profile, with the LCFS for typical and modified shaping on C-Mod shown.

The edge fibers have effective imaging spot sizes of approximately 1 mm at the outboard midplane; with typical pedestal widths of a few millimeters on C-Mod [20], this is sufficient spatial resolution to measure H-mode pedestals. However, the two 30 Hz lasers provide only a total 60 Hz cycle rate for the Thomson system, whereas ELMs on

C-Mod can exceed 100 Hz [6]; the ELMing discharges selected here typically exhibited ELMs of 60-100 Hz, comparable to the Thomson Scattering framerate. Nevertheless in these cases it is difficult to bin the pedestal data against the peaks of the ELM cycles immediately preceding the ELM crash, so for most discharges only ensemble-averaged measurements (described in section 2.3) are feasible. However, in longer steady ELMing periods there is sufficient ELM-cycle binned data to construct an ensemble of Thomson data taken only from ELM peaks.

In addition to Thomson Scattering temperature data, core and edge electron-cyclotron emission (ECE) T_e data are used for high time-resolution ELM diagnosis. Grating-polychromator ECE (GPC ECE) diagnostics [4] provide a total of 28 core and edge T_e channels with instrument-limited imaging sizes of ~ 9 mm, digitized at 20 kHz. Additionally, a high-resolution 32-channel heterodyne ECE (HRECE) diagnostic [21] provides plasma coverage with sub-centimeter spot sizes in the edge. Both have sufficient spatial resolution to distinguish edge T_e (though they cannot resolve the temperature pedestal structure), along with the time resolution necessary to track ELM crashes. T_e traces for both diagnostics are shown in figure 3.

2.3. Pedestal Modeling

The density and temperature pedestal data from the C-Mod Thomson Scattering systems are fitted using a modified hyperbolic-tangent function developed in Groebner *et al* [22]. For a general pedestal in x, y space, the fitting function is expressed by

$$y = \frac{b+h}{2} + \frac{h-b}{2}\mathrm{mtanh}\left(\alpha, z\right) \tag{1}$$

$$\mathrm{mtanh}\left(\alpha, z\right) = \frac{\left(1+\alpha z\right)e^{z} - e^{-z}}{e^{z}+e^{-z}} \tag{2}$$

$$z = \frac{x_0 - x}{\delta} \tag{3}$$

using x_0, h, b and δ as the pedestal midpoint, height, baseline, and half-width, respectively (we define $\Delta = 2\delta$ as the full width). The multiplicative factor $1 + \alpha z$ generates the approximately linear profile (characterized by α) within the core; this replaces the previous function used for C-Mod pedestal studies, which used a Heaviside step function for the core profile, with a function with a continuous gradient everywhere (however, this does not significantly alter the results of the fit).

Strictly, structural models in ELMing pedestals most closely correspond to the measured pedestal at the peaks of the ELM cycle, immediately preceding the crash. However, as noted in section 2.2, the ELM cycle on C-Mod is typically too rapid for the edge Thomson Scattering system to reliably resolve in all cases with multiple frames per ELM, complicating binning to the ELM cycle peaks. For certain discharges, a statistical set can be constructed from multiple ELMing discharges using binning to ELM cycle peaks. In most cases, however, we instead select periods of steady plasma behavior (density, stored energy, etc.) with consistent ELMs, and consider an "ensemble

average" (alternately termed the "ELM average") of the plasma pedestal. All Thomson Scattering data over such time periods are collated into a single ensemble-averaged pedestal for fitting, as shown in figure 2.

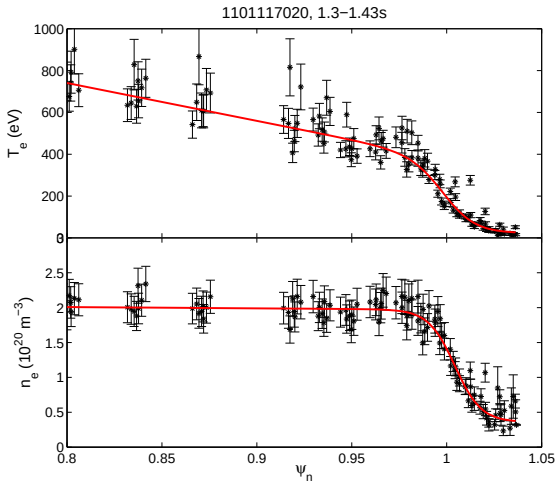

Figure 2: Electron temperature and density pedestals for C-Mod shot 1101117020, ensemble-averaged from 1.3-1.43s.

Sample H-mode traces from such an ELMing period for $\overline{n}_e$, core and edge T_e from ECE measurements, and H_α radiation are given in figure 3. The interior T_e measurement is taken from a GPC channel corresponding to $\sim 39\%$ of poloidal flux, just outside the inversion radius, cleanly displaying the sawtooth heat pulse. The edge ECE channel is taken from a HRECE channel corresponding to $\sim$ 97% of poloidal flux, near the pedestal top. Line-averaged density varies only slightly through the period (1.06-1.18s for the sample discharge shown), with minor dips corresponding to density expulsion with the ELM, while ELMs and the corresponding crashes in the edge T_e occur with consistent periods and amplitudes. The increase in T_e preceding the ELM crash, visible in figure 3b, is correlated to the core sawtooth heat pulse (visible on the interior ECE channel). Although this may (rather surprisingly) indicate that the ELM crash does not occur at peak edge T_e, comparison between ensemble-averaged and ELM-binned data (see figure 5) unambiguously shows the ELM crash occurring at peak pedestal pressure. This suggests a density effect, but current Thomson Scattering measurements on C-Mod do not have the necessary time resolution to track inter-elm pedestal evolution. This is a goal of future research.

Compared to a frame-by-frame average of the data, this method gives a minimal change in the result for well-converged fits, while preventing abnormal time frames from skewing the overall result for the ELMing period. An example of well-converged fits is given in figures 4a-4f. We use normalized poloidal flux for the abscissa, which both facilitates direct comparison to EPED results on DIII-D and corrects for shifts in the plasma position over the ELMing period.

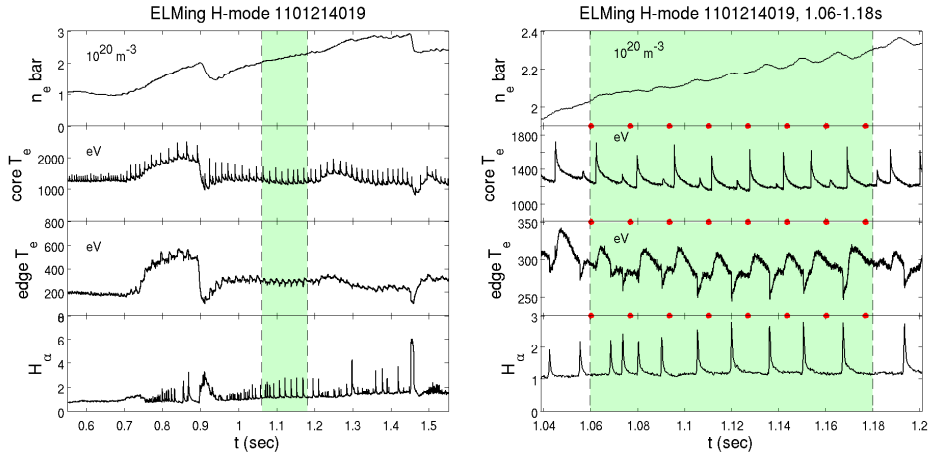

(a) H-mode trace. (b) ELMing time period traces.

Figure 3: ELMing H-mode traces, showing $\overline{n}_e$, core and edge ECE T_e, and H_α radiation traces for discharge 1101214019 (3a) and the ELMing period, 1.06-1.18s, selected for ensemble averaging (3b). Thomson data points are indicated by the red marks in figure 3b.

The peaks of the ELM cycle, corresponding to limiting thresholds in the pedestal structure, are found preceding the crashes in edge T_e and the corresponding spikes in H_α light. Typically, the ELM-synced pedestal structure is taken to be the last 20% of the time period preceding each ELM crash. A subset of the selected ELMing discharges with suitable measurements are also presented using ELM-cycle binned data for comparison with the ensemble-averaged result (see sections 3.2 and 5). At low pedestal pressures, ELMs on C-Mod are typically small enough that the ensemble-averaged pedestal differs little from the ELM-cycle synced result; at higher pressures (and thus larger ELMs), however, it is possible for the pedestal data to diverge significantly from the ensemble average. For the discharges prepared with ELM-cycle binned data, the pedestal pressures were on average 17.8% higher than the ensemble-averaged result, as shown in figure 5.

The fitted results for the pedestal width are taken as the average in flux space of the density and temperature pedestal widths,

$$\delta_\psi = \frac{\delta_n + \delta_T}{2} \qquad \Delta_\psi = 2\delta_\psi \tag{4}$$

in order to match to the outputs of the EPED model. Similarly constructing the pedestal pressure as $p = 2n_eT_e$ (alternately expressed by the poloidal beta at the pedestal top) allows direct comparison between the predicted ELMing pedestal and the observed result. While it is possible to directly fit the pressure pedestal width and height, use of the density/temperature average facilitates comparisons both between machines and with the model equilibria used in EPED. In practice, the results for the pedestal heights calculated by fitting the pressure pedestal versus taking $p_{ped} = 2n_{e,ped}T_{e,ped}$

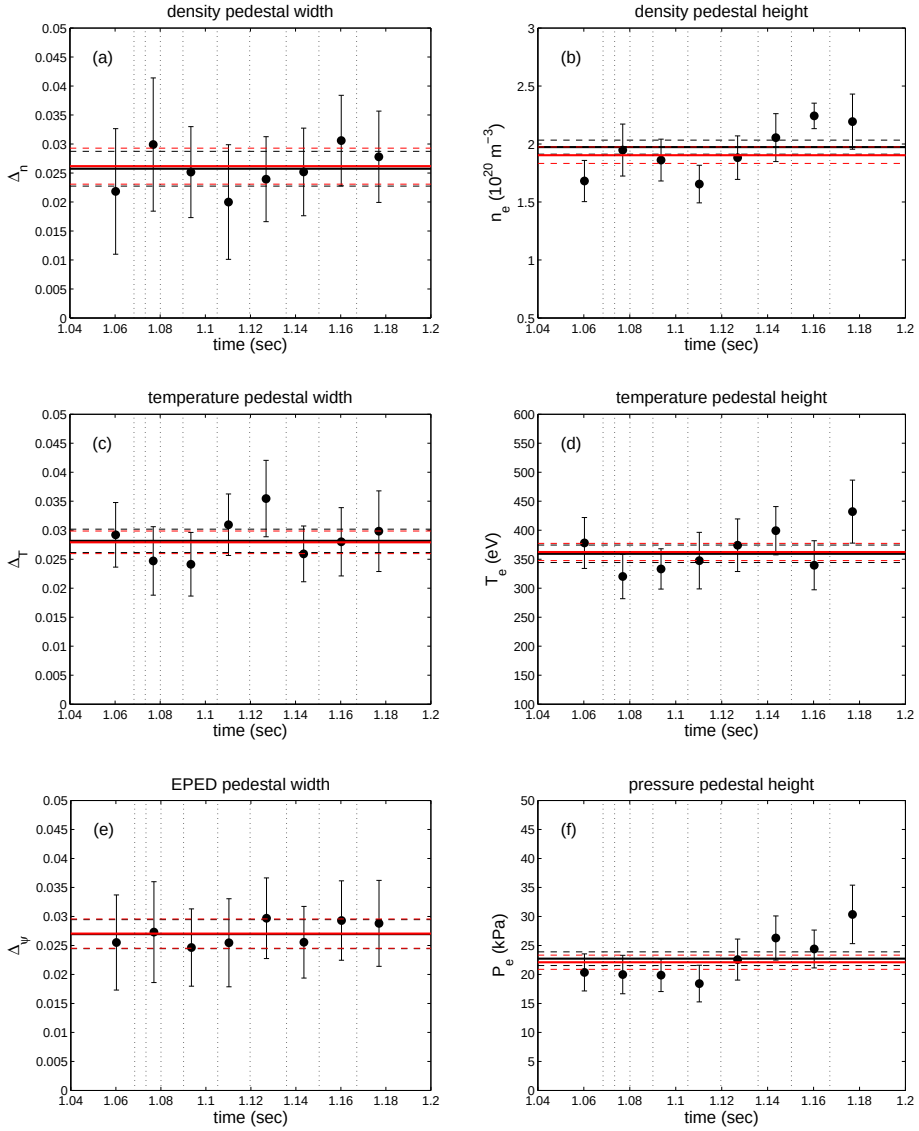

Figure 4: Comparison of time-frame-averaged fitting results to constructed ensemble fits for discharge 1101214019, 1.06-1.18 seconds. Time frame fitting results are shown as black points, with their average shown as the black line. The ensemble fit result is shown in red. For both the ensemble fit and the frame-averaged fit, the error bars are indicated by horizontal dashes. ELM times are indicated by the vertical dotted lines.

from density and temperature pedestals are quite similar. The pedestal width, being rather more difficult to measure, does vary between the two methods; however, the density/temperature average appears to mitigate some fitting errors, and retains a more rigorous match to the model.

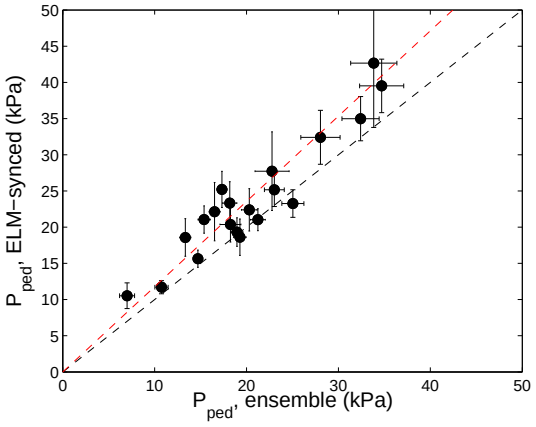

Figure 5: Comparison of the measured pedestal pressure for ensemble-averaged vs. ELM-syncronized pedestals. The black line indicates perfect agreement, while the red line shows the average 17.8% increase in measured pressure from ELM-cycle binning.

3. Experimental Results

The pedestal structure in C-Mod ELMing H-modes was explored across a broad range of operating parameters, including scans in plasma current (400-1100kA), toroidal magnetic field (3.5-8T on-axis), elongation ($1.4 < \kappa < 1.55$) and collisionality ($0.25 < \nu^* < 6$). A factor of seven variation in the pedestal pressure was observed across these discharges, while the pedestal width (measured in normalized poloidal flux) remained robust between 3 and 5%.

3.1. I_p scan

Previous scaling experiments on EDA H-modes [23] have demonstrated a robust linear dependence of the pedestal density $n_{e,ped}$ on the plasma current due to regulation of particle transport across the pedestal. A similar scaling is recovered in figure 6b; however, the dependence is less robust for ELMing H-modes than in the EDA case, with $n_{e,ped}$ less strictly controlled by I_p. While no clear dependence of $T_{e,ped}$ on I_p is seen (figure 6d), the pressure pedestal height p_{ped} (defined by $p_{ped} = 2n_{e,ped}T_{e,ped}$) reflects the clear linear scaling with I_p, shown in figure 6f. In high $T_{e,ped}$, low current (thus low collisionality) cases, as shown in figure 6d, the pedestal pressure can exceed the apparent linear dependence on I_p. Although the C-Mod pedestal width is robust across the parameter range (remaining within $3-5\%$ of normalized poloidal flux, shown in figure 6e), an inverse dependence with I_p is discernable. This, combined with the $p_{ped} \propto I_p$ scaling found above, is consistent with the $\nabla p \propto I_p^2$ scaling of the ETB pressure gradient, consistent with ballooning-limited pedestals, found in previous EDA scaling studies on C-Mod [23, 24, 25]; it has previously been suggested that C-Mod EDA H-Modes, DIII-D QH Modes, and ELMing H-Modes share similar critical-gradient limiting phenomena in their pedestals [9]. Notably, these studies of EDA H-modes on C-Mod

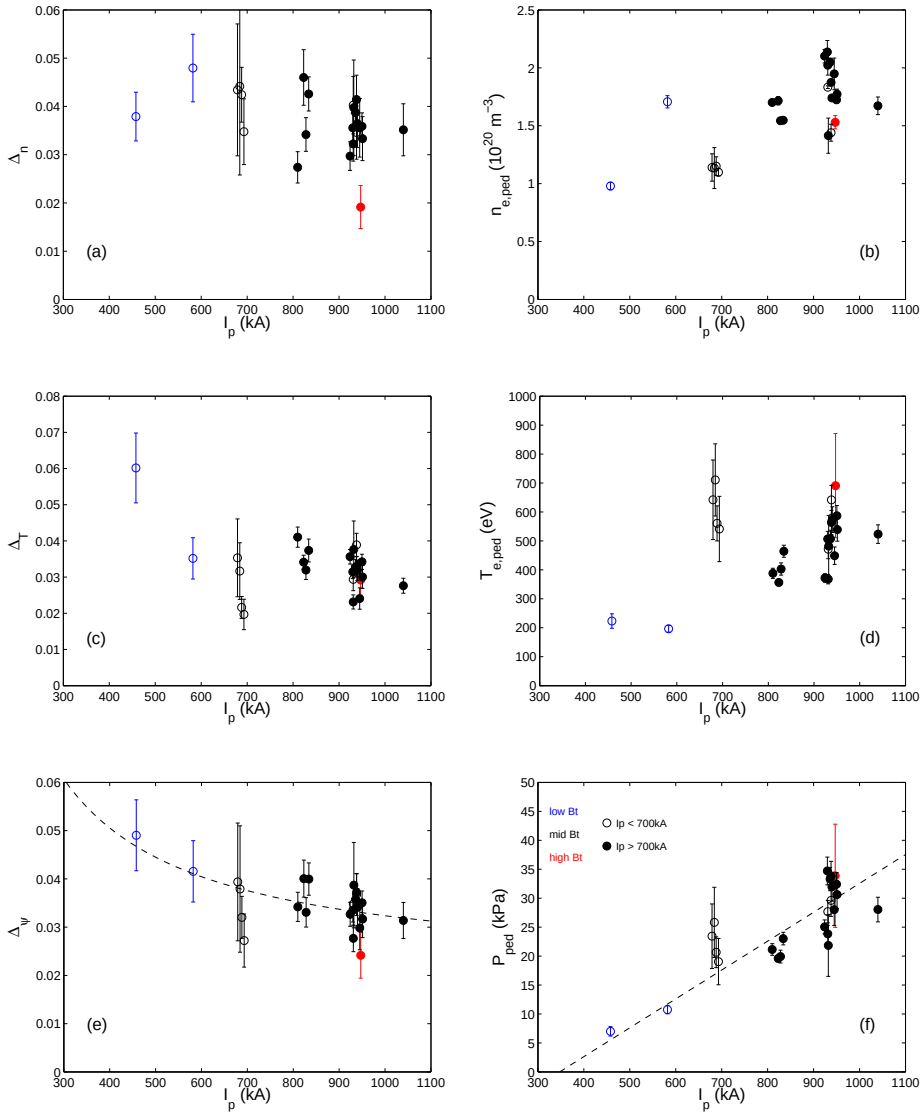

Figure 6: Plasma current scalings in density, temperature, and pressure pedestals. Low current ($I_p < 700$ kA) data are shown as open circles, while high current data are filled circles; 3.5T, 5.4T, and 8T data are shown in blue, black, and red respectively. $p_{ped} \propto I_p$ and $\Delta_\psi \propto I_p^{-1}$ dependencies are shown in figs. 6f and 6e.

found $p_{ped} \propto I_p^2$ with little scaling of the pedestal width with current; this, however, represents the soft limit found in EDA H-modes, rather than the saturated pedestal exhibiting $p_{ped} \propto I_p$ for ELMing discharges.

3.2. Width scalings

A scaling of the pedestal width with $\beta_{p,ped}$ has been observed [13, 9, 26], and shown to follow from a critical gradient limit on the edge pressure profile established by the kinetic ballooning mode or closely related instabilities [9, 10] . The expected dominant

scaling is $\Delta = c\beta_{p,ped}^{1/2}$, where c is a weakly varying function of a number of plasma parameters. As the ELMing H-modes from this experiment were rather restricted in the range of $\beta_{p,ped}$ available, older C-Mod discharges from 2006 used previous ELMing studies (e.g. [26]) were also implemented for β_p scalings, extending the available range below $\beta_{p,ped} \sim 0.1\%$. The measured pedestal width versus ensemble-averaged $\beta_{p,ped}$ is given in figure 7, with fitted scaled factor $\langle c \rangle = 0.088 \pm 0.01$.

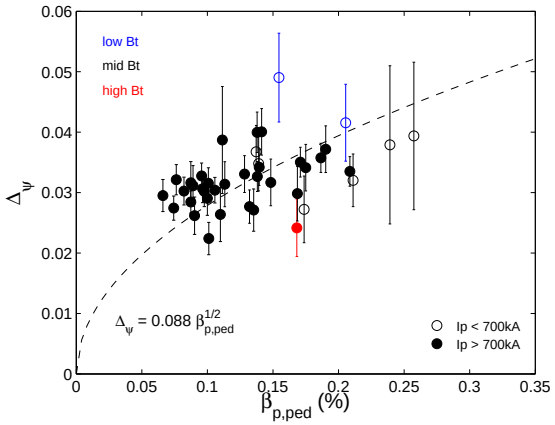

Figure 7: Ensemble-average xperimental scaling of Δ_ψ with $\beta_{p,ped}$. The scale factor c is found to be 0.088 ± 0.01. Low current ($I_p < 700$ kA) data are shown by open circles, while high current data are shown by filled circles. 3.5T, 5.4T, and 8T discharges are indicated in blue, black, and red respectively.

As noted in section 2.3, the EPED pedestal structure model is expected to correspond most precisely to measurements taken at the peaks of the ELM cycle, immediately preceding the ELM crash. A subset of the ELMing discharges presented here (including 2006 discharges) with suitable data were prepared with ELM-cycle synced data. Characteristic shifts, indicated by arrows, in $\beta_{p,ped}$ and Δ_ψ are shown in figure 8, along with fitted scalings with $\beta_{p,ped}^{1/2}$ for ensemble-averaged and ELM-synced pedestals.

Full analysis of the ELM-synced pedestals is given in figures 9a-9d. For figures 9a and 9b, ELM-synced shots (that is, a single pedestal from an ensemble of ELM-synced Thomson frames) were constructed. Figures 9c and 9d show individual ELM-synced Thomson frames instead. For additional statistical analysis, the data in both cases were prepared by averaging data points within fixed bins of values in $\beta_{p,ped}$ as well, shown in figures 9b and 9d (9a and 9c are raw data). For each, the pedestal data is fitted to the expected scaling $\Delta_\psi = c\beta_{p,ped}^{1/2}$, as well as the more general power law $\Delta = c_1\beta_{p,ped}^{c_2}$. The results of the fitting are given in table 1. Each is consistent with a $\beta_{p,ped}^{1/2}$ scaling for Δ_ψ, with a scale factor in the range $0.08 - 0.1$ consistent with previous experiment on C-Mod and DIII-D [26]. The fitting results are quite consistent across the four data analysis methods, showing that the $\Delta_\psi \propto \beta_{p,ped}^{1/2}$ scaling is remarkably insensitive to the exact model used.

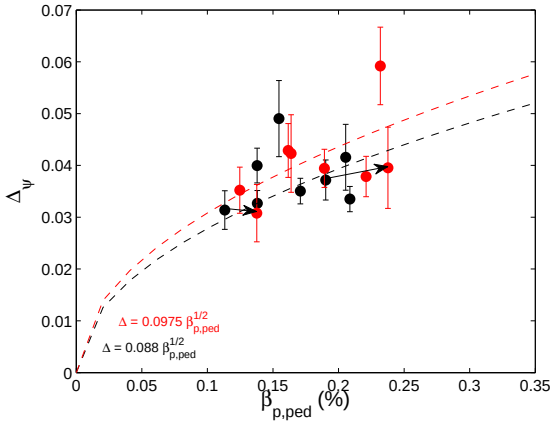

Figure 8: Experimental scaling of Δ_ψ with $\beta_{p,ped}$, showing characteristic shift in Δ_ψ and $\beta_{p,ped}$ between ensemble-averaged and ELM-synced pedestals. The scale factor c is found to be 0.088 ± 0.010 for the ensemble-averaged data, and 0.0975 ± 0.010 for ELM-cycle synced data (see table 1). Arrows indicate the shift from ensemble to ELM-synced data for two indicative discharges.

data	$\Delta_\psi = c_1 \beta_{p,ped}^{c_2}$		$\Delta_\psi = c\beta_{p,ped}^{1/2}$
	c_1	c_2	c
ELM-binned shots	0.0831 ± 0.03	0.42 ± 0.23	0.0975 ± 0.010
ELM-binned, β_p-binned shots	0.0923 ± 0.03	0.49 ± 0.20	0.0936 ± 0.015
ELM-binned frames	0.0833 ± 0.03	0.416 ± 0.15	0.0983 ± 0.010
ELM-binned, β_p-binned frames	0.0951 ± 0.03	0.51 ± 0.20	0.0941 ± 0.010

Table 1: Compilation of results from analysis methods for $\beta_{p,ped}$ vs. width scalings in ELM-binned discharges, fitting both $\Delta_\psi = c\beta_{p,ped}^{1/2}$ and $\Delta_\psi = c_1\beta_{p,ped}^{c_2}$.

Secondary scalings of the pedestal width may be discerned by normalizing the width to the dominant scaling $\Delta_\psi \propto c\beta_{p,ped}^{1/2}$, which has been well-characterized [9, 26], capturing variations in the factor c (more properly, a weakly varying function of ν^*, ρ^*, plasma shaping, etc.). Using a value of $c = 0.088$ from the ensemble-averaged data, variations in the pedestal width with the applied toroidal field B_T are shown in figure 10.

The high scatter in values for the normalized width at fixed values of B_T, along with the placement of the low- and high-field results within the range of scatter for the normal-field (5.4T) pedestals, indicates little systematic scaling of the Δ_ψ with B_T, although, given the difficulty in acquiring sufficient ELMing data at high fields, we cannot conclusively exclude a scaling of Δ_ψ with toroidal field independent of the dominant scaling with poloidal beta.

An alternate scaling argument for the pedestal width with ρ^* has been proposed [27], encapsulating an explicit B_T dependence with factors of ion mass, charge, and

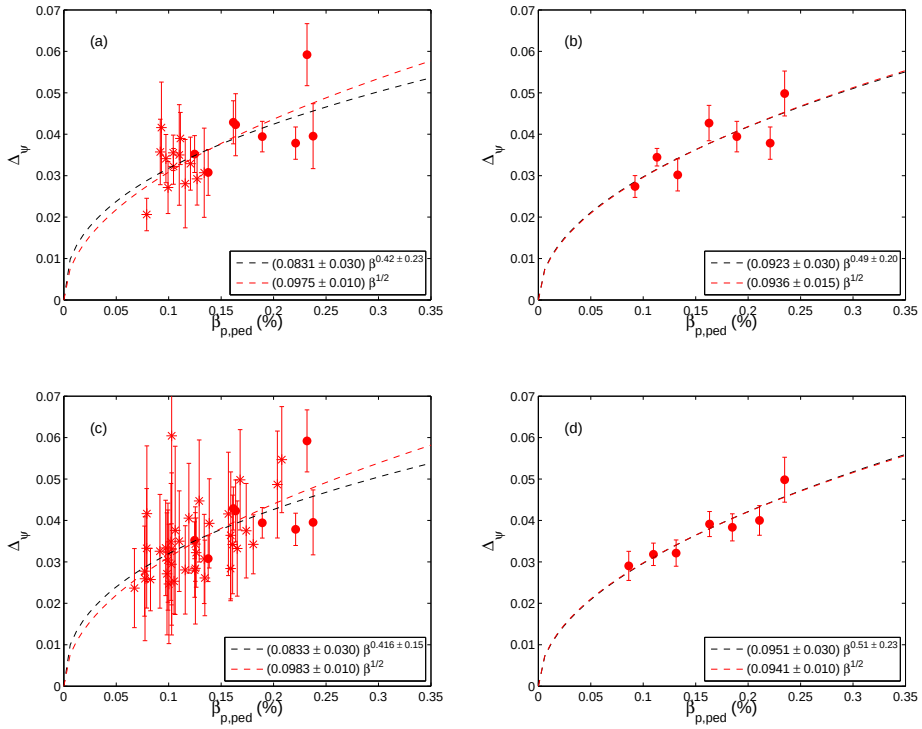

Figure 9: ELM-synced pedestal width vs. $\beta_{p,ped}$. 2006 discharges are shown by stars, and 2010/2011 discharges are indicated by circles. 9a shows ELM-synced discharges, with 9b showing the data averaged within bins of $\beta_{p,ped}$. 9c shows individual ELM-synced Thomson frames, with 9d showing the same binned in $\beta_{p,ped}$ as well. Each shows fitted curves for $\Delta_\psi = c\beta_{p,ped}^{1/2}$ and $\Delta_\psi = c_1\beta_{p,ped}^{c_2}$. The fitting results are given in table 1.

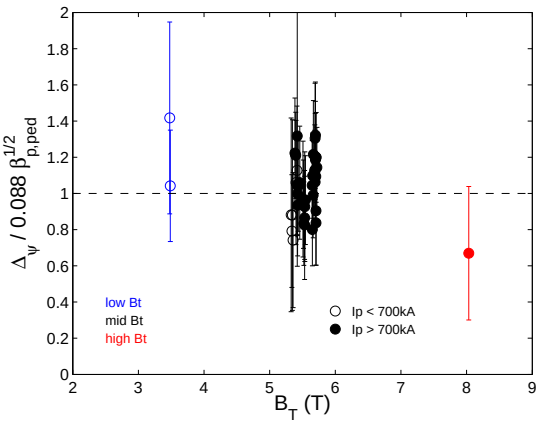

Figure 10: Scaling of the pedestal width Δ_ψ, normalized for the dominant scaling $\Delta_\psi = 0.088\beta_{p,ped}^{1/2}$, with the applied toroidal field B_T. Low current ($I_p < 700$ kA discharges are indicated by open circles, while high-current discharges are shown by filled circles.

temperature. Using

$$\rho^* = 4.6 \times 10^{-3} \frac{m^{1/2} \left(T_i \text{ [keV]}\right)^{1/2}}{ZaB_T} \tag{5}$$

where m is the primary ion mass in AMU and Z is the primary ion charge, the scaling of the normalized pedestal width with ρ^* is given in figure 11. Note that, given the lack of high spatial resolution ion temperature measurements in C-Mod pedestals, the electron temperature at the pedestal top was substituted.

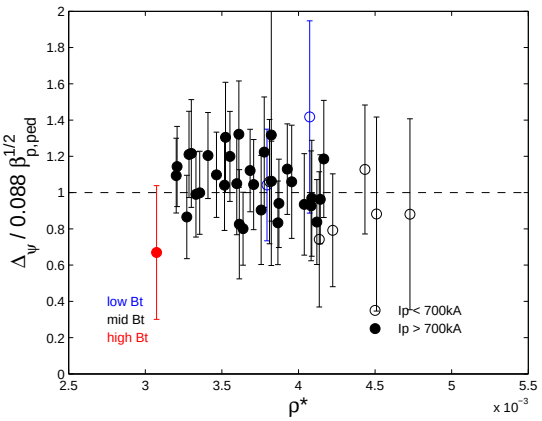

Figure 11: Secondary scaling of normalized pedestal width $\Delta_\psi/0.088\beta_{p,ped}^{1/2}$ with ρ^*. Low current ($I_p < 700$ kA) discharges are indicated by open circles, while high-current discharges are shown with filled circles. 3.5T, 5.4T, and 8T discharges are indicated by blue, black, and red respectively.

Across the accessible range of ρ^* in these ELMing pedestals, no systematic variation of the pedestal width (normalized for the $\beta_{p,ped}$ dependence) with ρ^* is seen, matching previous results from C-Mod [24] and ASDEX Upgrade [27].

Additional secondary scalings assumed for the scale factor c in κ and ν^*, using

$$\nu_e^* = 6.921 \times 10^{-18} \frac{Rq_{95}Z_{eff} \ln \Lambda_e}{\epsilon^{3/2} T_e^2} \tag{6}$$

from Oyama *et al* [28], are presented in figures 12a and 12b.
Little systematic variation in the normalized pedestal width is observed as collisionality is varied across a wide range (the high-ν^* values were obtained in cold, low-field discharges with pedestal temperatures of $\sim$ 150 eV). A similar result is observed for plasma shaping, across the range of κ available for ELMing discharges on C-Mod, consistent with previous pedestal studies.

4. The EPED Model

4.1. The Peeling-Ballooning Constraint

Pressure-gradient-driven ideal MHD ballooning modes in the edge were identified early on as a potential driver for edge-localized instabilities [13, 12]. However, this cannot

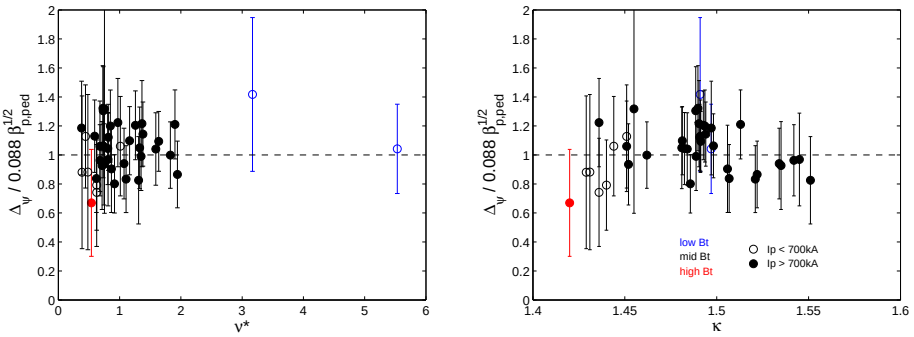

(a) ν^* scaling (b) κ scaling

Figure 12: Secondary parameter scalings of normalized pedestal width $\Delta_\psi/0.088\beta_{p,ped}^{1/2}$. Low current ($I_p < 700$ kA) discharges are indicated by open circles, while high-current discharges are shown with filled circles. 3.5T, 5.4T, and 8T discharges are indicated by blue, black, and red respectively.

satisfactorily explain all ELMing behaviors - for example, MHD analysis shows type III ELMs in C-Mod to be stable to the ideal ballooning mode [6, 20]. The incorporation of non-local, finite toroidal mode number (n) effects into MHD calculations brings in the current gradient terms which drive kink/peeling modes, and the complete set of intermediate to high-n instabilities are known as peeling-ballooning modes [8, 29, 7].

The combined peeling-ballooning model accounts for variation of the ELMing stability conditions with plasma shaping and collisionality: in low-collisionality regimes, low-n kink/peeling modes are the first to destabilize, while at high ν^* the bootstrap current is suppressed, and the discharge is limited by higher-n ($n \sim 10-30$) ballooning modes [8, 7, 26]. The model is further complicated at moderate ν^*, at which the peeling and ballooning modes can couple, producing large, dangerous current-driven instabilities [30]. The addition of bootstrap-current effects and diamagnetic stabilization allows pedestals to exceed the nominal ideal ballooning limit on the pedestal pressure gradient, an important effect on C-Mod [8, 20].

A number of MHD stability codes [31, 29, 32] have been used to study edge stability. The ELITE code [30, 8, 33], was designed specifically for this purpose, and calculates peeling-ballooning stability using an expansion in toroidal mode number at intermediate to high n, accounting for nonlocal effects. Studies of peeling-ballooning stability have been carried out on a number of machines and operational regimes, exploring dependencies on shaping [8, 29, 7], plasma beta [33], and collisionality [8, 7]. Through these, a variety of ELMs, as well as the EDA regime on C-Mod and the QH mode on DIII-D are found to exist at or below the peeling-ballooning boundary [9].

Most peeling-ballooning studies in experiments are interpretive, using measured equilibria to calculate stability boundaries. However, the EPED model is predictive, and so must be able to calculate this constraint before an experiment is conducted. It

does so using sets of carefully designed model equilibria in which the pedestal height is increased at a range of pedestal widths, to calculate a constraint on the pedestal height as a function of the pedestal width (usually characterized by normalized poloidal flux) [9, 26, 10]. Because the peeling-ballooning constraint on the pedestal height is a function of the width, it is insufficient by itself to uniquely predict pedestal height and width from engineering parameters, and so must be coupled to a second constraint.

4.2. The Kinetic-Ballooning Mode

In addition to the peeling-ballooning mode constraint, the EPED model considers the strong electromagnetic kinetic ballooning mode (KBM), the kinetic analogue to the MHD ballooning mode. The KBM drives strong turbulence in the pedestal despite the $E \times B$ shear turbulence suppression, effectively limiting pedestal growth. Gyrofluid and gyrokinetic calculations [34, 35, 36] identified the onset of the turbulence at a threshold correlated with the high-n ideal ballooning mode.

The onset of the KBM is quite stiff, allowing modeling of the turbulence onset as a threshold in the pedestal pressure gradient, which can be integrated across the pedestal to provide a second relationship between the pedestal height and width [9, 10]. Despite some similarities to the PBM, the KBM provides a distinct constraint on the pedestal width and height; an examination yields the strongest dependence with the square root of poloidal beta at the pedestal top, similar to observations on C-Mod [26] and DIII-D [13].

4.3. The EPED Model

The EPED model combines calculations of peeling-ballooning mode stability and KBM onset to yield a prediction of the pedestal height and width. Peeling-ballooning calculations are implemented using the ELITE code, which evaluates PBM stability on model equilibria constructed from a set of scalar input parameters [9]. Accounting for dependencies on other engineering parameters, the dominant scaling between pedestal width and height from the peeling-ballooning constraint is approximately $p_{ped} \sim \Delta_\psi^{3/4}$ [9, 26].

Calculations of kinetic ballooning mode onset note that the constrained width depends most strongly on the poloidal beta at the pedestal top, scaling as $\Delta_\psi \sim \beta_{p,ped}^{1/2}$ [10]. The onset condition is only weakly dependent on collisionality, shaping, safety factor, gyroradius, and beta - to good approximation, then, the KBM onset condition may be taken to be $\Delta_\psi = c\beta_{p,ped}^{1/2}$, where $c \approx 0.06 - 0.1$ is a weak function of the dimensionless parameters [9, 10].

In the current iteration of the model, EPED1.6, both the peeling-ballooning and kinetic-ballooning mode constraints are directly computed, yielding a fully first-principles predictive model for the pedestal structure. The peeling-ballooning constraint is calculated including an improved diamagnetic-stabilization model, particularly important for pedestal studies on C-Mod [10]. Likewise, the kinetic-ballooning

constraint is calculated for each case and accounts for the secondary dependencies of the onset condition with collisionality and shaping.

5. Comparison to Experiment

The EPED series of models has been tested extensively in ELMing scenarios across a number of machines. A dedicated experiment on C-Mod was conducted to test the implementation of a modified version of the model, EPED1.63 (a minor modification to EPED1.6 which calculates the KBM constraint at pedestal widths of 0.03 and 0.04, improving the robustness and efficiency of the model) across scans in plasma current (400-1000kA), magnetic field (3.5-8T), plasma shaping ($1.4 < \kappa < 1.6$), and collisionality ($0.25 < \nu^* < 6$), as detailed in section 2. The model is found to recover the observed pedestal widths and heights across the range of the parameter scans.

The improved diamagnetic stabilization model implemented in EPED1.63 is necessary to accurately predict the pedestal structure in C-Mod. The diamagnetic term is generally large in the C-Mod pedestal, and hence edge stability can be quite sensitive to it. Note that, while pedestal models most closely correspond to the measured pedestal shortly before an ELM, here data averaged across the full ELM cycle is used (as described in section 2.3). To evaluate the impact of this, for a subset of the ELMing discharges with suitable data, measurements binned to the last 20% of the ELM cycle were also prepared.

5.1. Pedestal Pressure

Pressure pedestal heights spanning a factor of seven variation were achieved in ELMing discharges. The measured pedestal pressure is plotted versus the EPED1.63 predicted pressure in figure 13, with perfect agreement indicated by the dashed line. Agreement is fairly good across the pedestal pressure range, with an average ratio of measured to predicted pedestal height of 0.84 ± 0.15. The accuracy of the model is similar to the $\sim$20% accuracy found in previous studies, though the predictions are systematically slightly high. We note that, on C-Mod, diamagnetic stabilization is quite strong, and modeling it accurately is paramount. Using slightly weaker diamagnetic stabilization brings the model into somewhat better agreement with the observations.

The small discrepancy between the measured and predicted pedestal heights may be partly attributed to using measurements averaged across the ELM cycle. Strictly, the EPED model calculates the stability threshold in the pedestal triggering the ELM, thus the EPED prediction most closely corresponds to the pedestal parameters immediately before the ELM crash. ELM-cycle binning (taking only pedestal data from the last $\sim$20% of the ELM cycle) typically gives closer correspondence to EPED predictions than full ELM-cycle averaging, but is often difficult on C-Mod due to the commonly rapid ELMs (see section 2.3). Although the ensemble-averaged pedestal pressure will generally be smaller than the pressure at the peaks of the ELM cycle, at lower pedestal

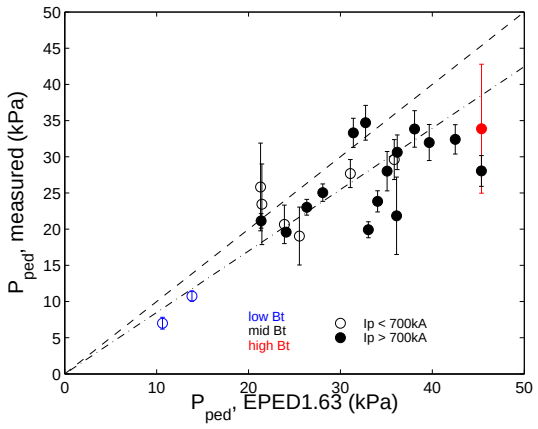

Figure 13: Measured pedestal pressure vs. EPED1.63 predicted pedestal pressure for 24 C-Mod discharges from dedicated ELMing runs over a wide range of plasma parameters. The dashed line indicates perfect agreement, while the dot-dash indicates the 1/1.178 line for the corrective factor between ensemble-averaged and ELM-synced pedestals (see figure 5). Low current ($I_p < 700$ kA) discharges are indicated by open circles, while high current discharges are shown by closed circles. 3.5T, 5.4T, and 8T data are shown in blue, black, and red respectively.

pressures the deviation between the two measurements is typically small, giving similar correspondence with the model prediction. It would similarly be expected that at higher pressures the deviation would be progressively worse (as is shown in figure 5), giving average measured pedestal pressures substantially below the predicted value, as is visible in figure 13 - a correlation line for the corrective factor $1/1.178 = 0.849$ found between the ensemble-averaged and ELM-synced pedestals in figure 5 is also shown. For a subset of the ELMing discharges presented here, it was possible to prepare ELM-cycle binned data; a comparison between the ensemble-averaged results for those discharges (indicated by the black points) and the ELM-cycle binned measurements (indicated in red) is given in figure 14.

ELM-cycle binning produces little variation from the ensemble-averaged result at low pressures, while presenting on average better correspondence to the EPED prediction at higher pressures (above $\sim$ 35 kPa). Across the data subset, the ratio of measured to predicted pedestal height for the binned data was 0.989 ± 0.15, compared to 0.84 for the ensemble-averaged result.

5.2. Pedestal Width

Pedestal width scalings are somewhat more challenging on C-Mod, given the generally robust width of the plasma pedestal (typically within 3-5% of the poloidal flux space corresponding to $\sim$ 5mm on C-Mod). The EPED model correctly recovers this robustness; a comparison of the measured versus predicted pedestal width, defined by Δ_ψ as given in (4).

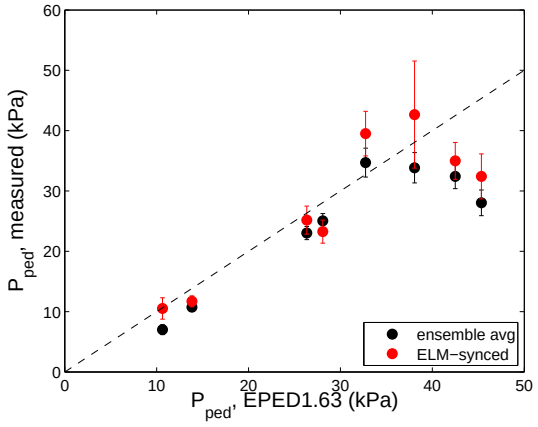

Figure 14: Measured pedestal pressure vs EPED1.63 predicted pedestal pressure. Black points indicate the ensemble-averaged data for a subset of the discharges, while red indicates the corresponding ELM-cycle-binned result.

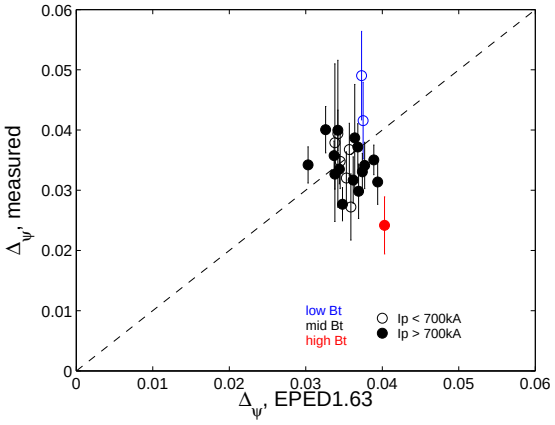

Figure 15: Measured pedestal width in normalized poloidal flux space vs. EPED1.63 predicted pedestal width for 24 C-Mod discharges from dedicated ELMing runs over a range of plasma parameters. The dashed line indicates perfect agreement. Low current ($I_p < 700$ kA) discharges are indicated by open circles, while high current discharges are shown by closed circles. 3.5T, 5.4T, and 8T data are shown in blue, black, and red respectively.

The model performs reasonably well, with a ratio of measured to predicted pedestal width of 1.01 ± 0.10, across parameter ranges from 3.5-8T in B_T and 400-1000kA in I_p. ELM-cycle binning, presented in figure 16 shows no systematic variation in the predicted widths, retaining the customarily robust pedestal widths on C-Mod.

The width predictions in the EPED models are based predominantly on a dependence of the pedestal width on $\beta_{p,ped}$, as described in section 3.2. While the newer versions of the EPED model account for minor variations of pedestal width with gyroradius, collisionality, and density, the dominant scaling is $\Delta \sim \beta_{p,ped}^{1/2}$, with a

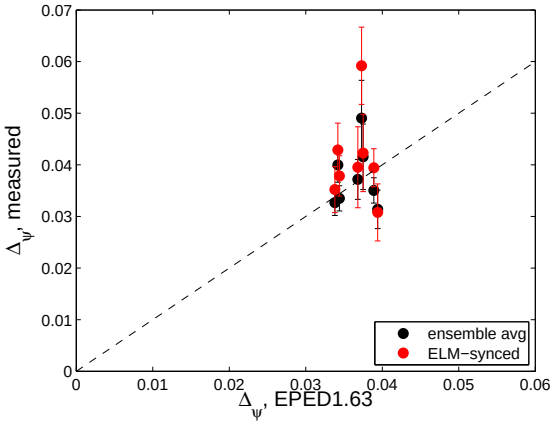

Figure 16: Measured pedestal width in normalized poloidal flux space vs. EPED1.63 predicted pedestal width. Red points indicate ELM-cycle binned data, while black points indicate ensemble-averaged widths for the corresponding discharges.

coefficient (more properly, a weakly varying function of ν^*, ρ^*, etc.) of ~ 0.08. The scale factor for the ELMing discharges presented here (using ensemble-averaged pedestals) was found to be $\langle c \rangle = 0.088 \pm 0.010$. The predicted and measured relations between Δ and $\beta_{p,ped}$ are given in figure 17. As noted in section 3.2, the range of available $\beta_{p,ped}$ in the discharges was rather limited; however, the EPED model is uniquely predicting values for both $\beta_{p,ped}$ and the width, so it remains a fairly stringent test of the model.

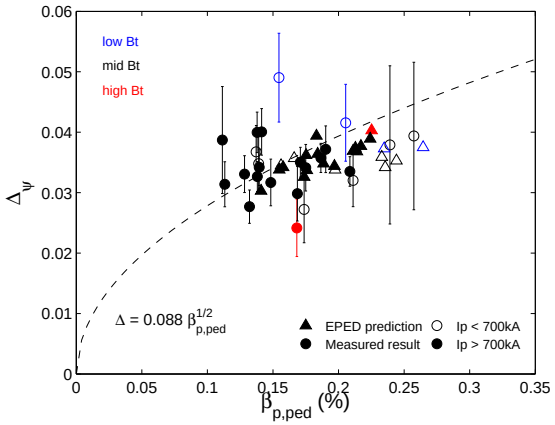

Figure 17: Pedestal width Δ vs. pedestal poloidal beta, $\beta_{p,ped}$. Circles indicate measured data, and triangles indicate EPED1.63 prediction. Low current ($I_p < 700$ kA) discharges are indicated by open points, while high current discharges are shown by filled points. 3.5T, 5.4T, and 8T data are shown in blue, black, and red respectively.

Overall trending with $\beta_{p,ped}^{1/2}$ is observed, although the experimental β_p measurements for ensemble-averaged pedestals at higher pressures skew lower than those predicted by EPED. This is corrected by ELM-cycle synchronized measurements, as shown in figures 8 and 9 in section 3.2.

6. Summary and Future Work

Experimental variation in the pedestal structure spanning a factor of seven variation in pressure pedestal height is consistent with a broad range of previously observed ETB phenomena in ELMing and EDA H-modes on C-Mod, indicative of underlying critical gradient phenomena limiting H-mode pedestals. While width comparisons were difficult given the robust pedestal width on C-Mod, a strong dependence of the pedestal width on $\beta_{p,ped}^{1/2}$ and weak or no dependence on other factors (B_T, ρ^*, ν^*, κ) was also recovered consistent with previous experiment.

Non-local peeling-ballooning stability of the edge barrier region is well-characterized by edge MHD stability codes such as ELITE. The EPED model combines this non-local peeling ballooning constraint with an integrated local kinetic ballooning mode constraint to predict the pedestal height and width, yielding a pedestal width which scales approximately as $\beta_{p,ped}^{1/2}$. The newest version of the code, EPED1.6, includes a direct calculation of the kinetic-ballooning mode constraint for each case, in addition to an improved model for diamagnetic stabilization of peeling-ballooning modes [10]. EPED1.63, a minor alteration of EPED1.6 optimized for C-Mod.

Overall agreement between the EPED1.63 predictions and observed pedestal structure in the C-Mod discharges was fairly good, with a ratio of measured to predicted pedestal height of 0.84 ± 0.15 and a ratio of predicted to measured pedestal width of 1.01 ± 0.08. Notably, the pressure pedestal height was consistently slightly low compared to the EPED prediction. This was likely due to the measurement method for the experimental pedestals: as ELMs on C-Mod are frequently too rapid for the Thomson Scattering system to reliably image with multiple frames per ELM, it proves more straightforward to construct ensemble-averaged pedestals from steady ELMing periods. Strictly, the stability model used in EPED corresponds to the pedestal immediately preceding the ELM crash; including pedestal data from outside this ELM-synchronized period should give systematically low pressure pedestal heights compared to prediction, with the divergence growing at larger pressures (corresponding to larger ELMs). Successful ELM-cycle synchronization on a subset of the discharges yielded better correspondence with the EPED predictions, with a ratio of measured to predicted pedestal height of 0.989 ± 0.15. Likewise, the ELM-cycle binned measurements reproduced the rough KBM scaling $\Delta = c\beta_{p,ped}^{1/2}$ with $\langle c \rangle \approx 0.09$, varying slightly with the exact analysis method used, as shown in figure 9 (compared to the previously observed result of $\langle c \rangle \approx 0.084$ on C-Mod), while the ensemble-averaged pedestals found $\langle c \rangle = 0.088 \pm 0.01$.

In addition, the importance of diamagnetic stabilization in C-Mod pedestals warrants further testing of the diamagnetic stabilization model implemented in EPED1.63. The planned upgrade of the Thomson Scattering system on C-Mod will increase the suitability of pedestal data for ELM-cycle synchronization, allowing ongoing validation of the EPED model series on C-Mod plasmas.

Acknowledgments

The authors wish to acknowledge the support of the C-Mod technical staff and machine operators. This work was supported by US Department of Energy Agreement DE-FC02-99ER54512.

References

[1] F. Wagner, G. Becker, K. Behringer, D. Campbell, A. Eberhagen, W. Engelhardt, G. Fussmann, O. Gehre, J. Gernhardt, G. v. Gierke, G. Haas, M. Huang, F. Karger, M. Keilhacker, O. Klüber, M. Kornherr, K. Lackner, G. Lisitano, G. G. Lister, H. M. Mayer, D. Meisel, E. R. Müller, H. Murmann, H. Niedermeyer, W. Poschenrieder, H. Rapp, H. Röhr, F. Schneider, G. Siller, E. Speth, A. Stäbler, K. H. Steuer, G. Venus, O. Vollmer, and Z. Yü. Regime of improved confinement and high beta in neutral-beam-heated divertor discharges of the asdex tokamak. *Phys. Rev. Lett.*, 49(19):1408–1412, Nov 1982.

[2] E.J. Doyle, W.A. Houlberg, Y. Kamada, V. Mukhovatov, T.H. Osborne, A. Polevoi, G. Bateman, J.W. Connor, J.G. Cordey, T. Fujita, X. Garbet, T.S. Hahm, L.D. Horton, A.E. Hubbard, F. Imbeaux, F. Jenko, J.E. Kinsey, Y. Kishimoto, J. Li, T.C. Luce, Y. Martin, M. Ossipenko, V. Parail, A. Peeters, T.L. Rhodes, J.E. Rice, C.M. Roach, V. Rozhansky, F. Ryter, G. Saibene, R. Sartori, A.C.C. Sips, J.A. Snipes, M. Sugihara, E.J. Synakowski, H. Takenaga, T. Takizuka, K. Thomsen, M.R. Wade, H.R. Wilson, ITPA Transport Physics Topical Group, ITPA Confinement Database, Modelling Topical Group, ITPA Pedestal, and Edge Topical Group. Chapter 2: Plasma confinement and transport. *Nuclear Fusion*, 47(6):S18, 2007.

[3] M. Greenwald, R.L. Boivin, F. Bombarda, P.T. Bonoli, C.L. Fiore, D. Garnier, J.A. Goetz, S.N. Golovato, M.A. Graf, R.S. Granetz, S. Horne, A. Hubbard, I.H. Hutchinson, J.H. Irby, B. LaBombard, B. Lipschultz, E.S. Marmar, M.J. May, G.M. McCracken, P. O'Shea, J.E. Rice, J. Schachter, J.A. Snipes, P.C. Stek, Y. Takase, J.L. Terry, Y. Wang, R. Watterson, B. Welch, and S.M. Wolfe. H mode confinement in alcator c-mod. *Nuclear Fusion*, 37(6):793, 1997.

[4] A. E. Hubbard, R. L. Boivin, R. S. Granetz, M. Greenwald, I. H. Hutchinson, J. H. Irby, Y. In, J. Kesner, B. LaBombard, Y. Lin, J. E. Rice, T. Sunn Pedersen, J. A. Snipes, P. C. Stek, Y. Takase, S. M. Wolfe, and S. Wukitch. Measurements of the high confinement mode pedestal region on alcator c-mod. *Physics of Plasmas*, 5(5):1744–1751, 1998.

[5] M Keilhacker, G Becker, K Bernhardi, A Eberhagen, M ElShaer, G FuBmann, O Gehre, J Gernhardt, G v Gierke, E Glock, G Haas, F Karger, S Kissel, O Kluber, K Kornherr, K Lackner, G Lisitano, G G Lister, J Massig, H M Mayer, K McCormick, D Meisel, E Meservey, E R Muller, H Murmann, H Niedermeyer, W Poschenrieder, H Rapp, B Richter, H Rohr, F Ryter, F Schneider, S Siller, P Smeulders, F Soldner, E Speth, A Stabler, K Steinmetz, K-H Steuer, Z Szymanski, G Venus, O Vollmer, and F Wagner. Confinement studies in l and h-type asdex discharges. *Plasma Physics and Controlled Fusion*, 26(1A):49, 1984.

[6] D. A. Mossessian, P. Snyder, A. Hubbard, J. W. Hughes, M. Greenwald, B. LaBombard, J. A. Snipes, S. Wolfe, and H. Wilson. High-confinement-mode edge stability of alcator c-mod plasmas. *Physics of Plasmas*, 10(5):1720–1726, 2003.

[7] H R Wilson, S C Cowley, A Kirk, and P B Snyder. Magneto-hydrodynamic stability of the h-mode transport barrier as a model for edge localized modes: an overview. *Plasma Physics and Controlled Fusion*, 48(5A):A71, 2006.

[8] P. B. Snyder, H. R. Wilson, J. R. Ferron, L. L. Lao, A. W. Leonard, T. H. Osborne, A. D. Turnbull, D. Mossessian, M. Murakami, and X. Q. Xu. Edge localized modes and the pedestal: A model based on coupled peeling–ballooning modes. *Physics of Plasmas*, 9(5):2037–2043, 2002.

[9] P. B. Snyder, R. J. Groebner, A. W. Leonard, T. H. Osborne, and H. R. Wilson. Development

and validation of a predictive model for the pedestal height. *Physics of Plasmas*, 16(5):056118, 2009.

[10] P.B. Snyder, R.J. Groebner, J.W. Hughes, T.H. Osborne, M. Beurskens, A.W. Leonard, H.R. Wilson, and X.Q. Xu. A first-principles predictive model of the pedestal height and width: development, testing and iter optimization with the eped model. *Nuclear Fusion*, 51(10):103016, 2011.

[11] Y. Lin, J. Irby, P. Stek, I. Hutchinson, J. Snipes, R. Nazikian, and M. McCarthy. Upgrade of reflectometry profile and fluctuation measurements in alcator c-mod. *Review of Scientific Instruments*, 70(1):1078–1081, 1999.

[12] W Suttrop. The physics of large and small edge localized modes. *Plasma Physics and Controlled Fusion*, 42(5A):A1, 2000.

[13] T H Osborne, R J Groebner, L L Lao, A W Leonard, R Maingi, R L Miller, G D Porter, D M Thomas, and R E Waltz. H-mode pedestal characteristics, elms, and energy confinement in iter shape discharges on diii-d. *Plasma Physics and Controlled Fusion*, 40(5):845, 1998.

[14] D A Mossessian, P B Snyder, M Greenwald, J W Hughes, Y Lin, A Mazurenko, S Medvedev, H R Wilson, and S Wolfe. H-mode pedestal characteristics and mhd stability of the edge plasma in alcator c-mod. *Plasma Physics and Controlled Fusion*, 44(4):423, 2002.

[15] S Saarelma, A Alfier, M N A Beurskens, R Coelho, H R Koslowski, Y Liang, I Nunes, and JET EFDA contributors. Mhd stability analysis of small elm regimes in jet. *Plasma Physics and Controlled Fusion*, 51(3):035001, 2009.

[16] J W Connor. Edge-localized modes - physics and theory. *Plasma Physics and Controlled Fusion*, 40(5):531, 1998.

[17] J.W. Hughes, A. Loarte, M.L. Reinke, J.L. Terry, D. Brunner, M. Greenwald, A.E. Hubbard, B. LaBombard, B. Lipschultz, Y. Ma, S. Wolfe, and S.J. Wukitch. Power requirements for superior h-mode confinement on alcator c-mod: experiments in support of iter. *Nuclear Fusion*, 51(8):083007, 2011.

[18] J. W. Hughes, D. A. Mossessian, A. E. Hubbard, E. S. Marmar, D. Johnson, and D. Simon. High-resolution edge thomson scattering measurements on the alcator c-mod tokamak. *Review of Scientific Instruments*, 72(1):1107–1110, 2001.

[19] J. W. Hughes, D. Mossessian, K. Zhurovich, M. DeMaria, K. Jensen, and A. Hubbard. Thomson scattering upgrades on alcator c-mod. *Review of Scientific Instruments*, 74(3):1667–1670, 2003.

[20] A E Hubbard. Physics and scaling of the h-mode pedestal. *Plasma Physics and Controlled Fusion*, 42(5A):A15, 2000.

[21] J. W. Heard, C. Watts, R. F. Gandy, P. E. Phillips, G. Cima, R. Chatterjee, A. Blair, A. Hubbard, C. W. Domier, and N. C. Luhmann. High resolution electron cyclotron emission temperature profile and fluctuation diagnostic for alcator c-mod. *Review of Scientific Instruments*, 70(1):1011–1013, 1999.

[22] R.J. Groebner, D.R. Baker, K.H. Burrell, T.N. Carlstrom, J.R. Ferron, P. Gohil, L.L. Lao, T.H. Osborne, D.M. Thomas, W.P. West, J.A. Boedo, R.A. Moyer, G.R. McKee, R.D. Deranian, E.J. Doyle, C.L. Rettig, T.L. Rhodes, and J.C. Rost. Progress in quantifying the edge physics of the hmode regime in diii-d. *Nuclear Fusion*, 41(12):1789, 2001.

[23] J.W. Hughes, B. LaBombard, J. Terry, A. Hubbard, and B. Lipschultz. Edge profile stiffness and insensitivity of the density pedestal to neutral fuelling in alcator c-mod edge transport barriers. *Nuclear Fusion*, 47(8):1057, 2007.

[24] J. W. Hughes, A. E. Hubbard, D. A. Mossessian, B. LaBombard, T. M. Biewer, R. S. Granetz, M. Greenwald, I. H. Hutchinson, J. H. Irby, Y. Lin, E. S. Marmar, M. Porkolab, J. E. Rice, J. A. Snipes, J. L. Terry, S. Wolfe, and K. Zhurovich. H-mode pedestal and l-h transition studies on alcator c-mod. *Fusion Science and Technology*, 51(3):317–341, 2007.

[25] J. W. Hughes, D. A. Mossessian, A. E. Hubbard, B. LaBombard, and E. S. Marmar. Observations and empirical scalings of the high-confinement mode pedestal on alcator c-mod. *Physics of Plasmas*, 9(7):3019–3030, 2002.

[26] P.B. Snyder, N. Aiba, M. Beurskens, R.J. Groebner, L.D. Horton, A.E. Hubbard, J.W. Hughes, G.T.A. Huysmans, Y. Kamada, A. Kirk, C. Konz, A.W. Leonard, J. Lnnroth, C.F. Maggi, R. Maingi, T.H. Osborne, N. Oyama, A. Pankin, S. Saarelma, G. Saibene, J.L. Terry, H. Urano, and H.R. Wilson. Pedestal stability comparison and iter pedestal prediction. *Nuclear Fusion*, 49(8):085035, 2009.

[27] M. N. A. Beurskens, T. H. Osborne, P. A. Schneider, E. Wolfrum, L. Frassinetti, R. Groebner, P. Lomas, I. Nunes, S. Saarelma, R. Scannell, P. B. Snyder, D. Zarzoso, I. Balboa, B. Bray, M. Brix, J. Flanagan, C. Giroud, E. Giovannozzi, M. Kempenaars, A. Loarte, E. de la Luna, G. Maddison, C. F. Maggi, D. McDonald, R. Pasqualotto, G. Saibene, R. Sartori, Emilia R. Solano, M. Walsh, L. Zabeo, , and and. H-mode pedestal scaling in diii-d, asdex upgrade, and jet. *Physics of Plasmas*, 18(5):056120, 2011.

[28] N Oyama, P Gohil, L D Horton, A E Hubbard, J W Hughes, Y Kamada, K Kamiya, A W Leonard, A Loarte, R Maingi, G Saibene, R Sartori, J K Stober, W Suttrop, H Urano, W P West, and the ITPA Pedestal Topical Group. Pedestal conditions for small elm regimes in tokamaks. *Plasma Physics and Controlled Fusion*, 48(5A):A171, 2006.

[29] G T A Huysmans. Elms: Mhd instabilities at the transport barrier. *Plasma Physics and Controlled Fusion*, 47(12B):B165, 2005.

[30] H. R. Wilson, P. B. Snyder, G. T. A. Huysmans, and R. L. Miller. Numerical studies of edge localized instabilities in tokamaks. *Physics of Plasmas*, 9(4):1277–1286, 2002.

[31] G. T. A. Huysmans, S. E. Sharapov, A. B. Mikhailovskii, and W. Kerner. Modeling of diamagnetic stabilization of ideal magnetohydrodynamic instabilities associated with the transport barrier. *Physics of Plasmas*, 8(10):4292–4305, 2001.

[32] S Yu Medvedev, A A Martynov, Y R Martin, O Sauter, and L Villard. Edge kink/ballooning mode stability in tokamaks with separatrix. *Plasma Physics and Controlled Fusion*, 48(7):927, 2006.

[33] P.B. Snyder, K.H. Burrell, H.R. Wilson, M.S. Chu, M.E. Fenstermacher, A.W. Leonard, R.A. Moyer, T.H. Osborne, M. Umansky, W.P. West, and X.Q. Xu. Stability and dynamics of the edge pedestal in the low collisionality regime: physics mechanisms for steady-state elm-free operation. *Nuclear Fusion*, 47(8):961, 2007.

[34] P. B. Snyder and G. W. Hammett. Electromagnetic effects on plasma microturbulence and transport. *Physics of Plasmas*, 8(3):744–749, 2001.

[35] Bruce D Scott. Computation of electromagnetic turbulence and anomalous transport mechanisms in tokamak plasmas. *Plasma Physics and Controlled Fusion*, 45(12A):A385, 2003.

[36] F Jenko and W Dorland. Nonlinear electromagnetic gyrokinetic simulations of tokamak plasmas. *Plasma Physics and Controlled Fusion*, 43(12A):A141, 2001.